M&C 2017 - International Conference on Mathematics & Computational Methods Applied to Nuclear Science & Engineering, Jeju, Korea, April 16-20, 2017, on USB (2017)

Energy-Dependent Implicit Filtered P_N Method for Thermal Radiation Transport

Vincent M. Laboure,* Ryan G. McClarren*

*Department of Nuclear Engineering, Texas A&M University, College Station, TX 77843–3133
vincent.laboure@tamu.edu, rgm@tamu.edu

Abstract - *In this work, we extend the Implicit Filtered P_N method to energy-dependent problems in the context of Thermal Radiation Transport. First, we derive temperature-dependent multigroup opacities using a power regression of the model opacity from [1]. Second, we propose a methodology to adjust the group-dependent filter strengths relying on Planck-weighting. Several spatial filtering strategies are then studied in terms of accuracy and computational cost. Spatially local strategies tend to be preferable though determining the spatial dependency of the filter may require more tuning than for uniform strategies. Overall, filtering improves the conditioning of the linear system.*

I. INTRODUCTION

A great deal of effort has been dedicated towards the development of numerical methods to simulate the thermal radiation transport (TRT) equations, which govern the propagation of photons and their interaction with the surrounding material. An option for the angular discretization is to use the spherical harmonics – or P_N – approximation to express the photon angular intensity Ψ using a spherical harmonics expansion, truncated up to a given order N.

While this method spectrally converges to the analytical solution and ensures rotational invariance, a major issue is its proneness to approximate rapidly varying functions in angle with highly oscillatory solutions. Typically, this may even induce regions where Ψ reaches negative values, which is – of course – nonphysical. Worse yet, the material temperature T can then suffer from that same problem, in which case the planckian re-emission terms become nonsensical.

The Filtered P_N ($\mathrm{F}P_N$) method aims at mitigating this very flaw. It was first proposed by McClarren and Hauck [2] as a conservative fix penalizing the higher derivatives in angle while preserving the rotational invariance of the solution. Other formulations were later developed to further reduce the impact of the Gibbs phenomena on the solution [3]. A significant step forward was achieved in [4] showing a convenient way to recast this filtering approach through an additional collision operator directly in the transport equation. While all these methods require the user to choose the strength of the filter, this last formulation no longer requires to adjust it as the spatial and temporal meshes are refined, thus allowing to tune it on coarse meshes. In [5], this method was studied in the context of time-implicit discretization schemes, so crucial for TRT applications given that the photons travel at the speed of light and therefore that the Courant-Friedrich-Lewy condition imposes to use minuscule times steps for explicit schemes. It was in particular found that the implicit filter improves the conditioning of the linear system in the streaming limit. This implies that the computational cost of the method tends to be reduced by the filter. It was also found that allowing the filter strength to be spatially dependent may yield a more accurate solution for a given N.

The study however was limited to the energy-integrated form of the TRT equations. In this work, we wish to study this method in the context of multigroup calculations with temperature dependent opacities. We study how the energy-dependent filter strength may be chosen and how it affects the computational cost of the method.

II. THEORY

In this paper, we consider the TRT equations which consists of the linear Boltzmann equation coupled with the material energy equation. We first briefly detail these equations and then describe the model opacity that we choose for the material.

1. Multigroup Thermal Radiation Transport

The energy structure is decomposed into G groups, the g-th corresponding to the energy interval $[E_{g-1}, E_g] = [h\nu_{g-1}, h\nu_g]$, where h is the Planck constant and ν is the photon frequency. The multigroup TRT equations are obtained upon integration of the linear Boltzmann equation over each energy group. It then states that for all energy group g, $1 \leq g \leq G$:

$$\begin{aligned}&\frac{1}{c}\frac{\partial \Psi_g}{\partial t} + \boldsymbol{\Omega}\cdot\boldsymbol{\nabla}\Psi_g + \sigma_{t,g}(\boldsymbol{r},T)\Psi_g(\boldsymbol{r},T)\\ &= \sigma_g(\boldsymbol{r},T)B_g(T) + \int_{4\pi}\sigma_{s,g}(\boldsymbol{r},\boldsymbol{\Omega}'\cdot\boldsymbol{\Omega})\Psi_g(\boldsymbol{r},\boldsymbol{\Omega}')\,\mathrm{d}\Omega' + S_g,\end{aligned} \tag{1a}$$

and

$$C_v\frac{\partial T}{\partial t} = \sum_{g=1}^{G}\sigma_g(\boldsymbol{r},T)(\Phi_g - 4\pi B_g(T)). \tag{1b}$$

In these equations, Ψ_g represent the photon angular intensity, S_g the volumetric source; $\sigma_{t,g}$, σ_g and $\sigma_{s,g}$ are respectively the total, absorption and scattering multigroup opacities; C_v is the material heat capacity and T is the material temperature. Also, Φ_g designates the scalar intensity defined as:

$$\Phi_g \equiv \int_{4\pi}\Psi_g \mathrm{d}\Omega. \tag{2}$$

Furthermore, the Planckian is:

$$B_g(T) \equiv \int_{\nu_{g-1}}^{\nu_g} B_\nu(\nu,T)\,\mathrm{d}\nu, \tag{3}$$

where the frequency-dependent Planckian B_ν is defined as:

$$B_\nu(\nu, T) \equiv \frac{2h\nu^3}{c^2} \frac{1}{\exp\left(\frac{h\nu}{kT}\right) - 1}, \tag{4}$$

c and k being respectively the speed of light in vacuum and the Boltzmann constant.

This physics is very relevant to the study of Filtered P_N methods because if T reaches negative values, B_ν is not integrable over $[0, \infty)$.

2. Model Opacity

We consider a pure absorber problem – without loss of generality – and choose the following energy-dependent and temperature-dependent model opacity used in [1] (Eq. (69) of that work):

$$\sigma(\boldsymbol{r}, \nu, T) = \sigma_0(\boldsymbol{r}) \frac{1 - \exp(-h\nu/kT)}{(h\nu)^3}, \tag{5}$$

the profile for $\sigma_0(\boldsymbol{r})$ being later chosen as illustrated in Fig. 1. As explained in [1], this model presents two realistic features: the value for $h\nu \ll kT$ is much larger than for $h\nu > kT$ and it decreases as T increases for fixed $h\nu$. We construct the multigroup opacities by taking its Rosseland-average:

$$\sigma_g(\boldsymbol{r}, T) \equiv \frac{\int_{\nu_{g-1}}^{\nu_g} \frac{\partial B_\nu}{\partial T} \mathrm{d}\nu}{\int_{\nu_{g-1}}^{\nu_g} \frac{1}{\sigma} \frac{\partial B_\nu}{\partial T} \mathrm{d}\nu}. \tag{6}$$

3. Implicit Filtered P_N

Using the P_N approximation, we have:

$$\Psi_g(\boldsymbol{r}, \boldsymbol{\Omega}) \approx \mathbf{R}^T(\boldsymbol{\Omega})\, \boldsymbol{\Phi}_g(\boldsymbol{r}) = \sum_{\ell=0}^{N} \sum_{m=-\ell}^{\ell} \Phi_{\ell,g}^m(\boldsymbol{r})\, R_\ell^m(\boldsymbol{\Omega}), \tag{7}$$

where the real-form spherical harmonics are defined as:

$$R_\ell^m(\boldsymbol{\Omega}) = \begin{cases} \sqrt{2}\, C_\ell^m\, P_\ell^m(\mu) \cos(m\varphi), & 0 < m \leq \ell \leq N \\ C_\ell^0\, P_\ell^0(\mu), & 0 \leq \ell \leq N \\ \sqrt{2}\, C_\ell^{|m|}\, P_\ell^{|m|}(\mu) \sin(|m|\varphi), & 0 < -m \leq \ell \leq N \end{cases}, \tag{8}$$

P_ℓ^m designating the associated Legendre polynomial of degree ℓ and order m and $C_\ell^m = \sqrt{\frac{(2\ell+1)}{4\pi} \frac{(\ell-m)!}{(\ell+m)!}}$ being a normalization constant chosen such that the spherical harmonics are orthonormal to each other.

The P_N equations are obtained by multiplying Eq. (1a) with the vector of the spherical harmonics $\mathbf{R}$ and integrating over the unit sphere. We choose the Backward Euler time-integration scheme, without loss of generality. Adding the filtering operator to the equation then yields, for all $g \in \{1, ..., G\}$:

$$\frac{\boldsymbol{\Phi}_g - \boldsymbol{\Phi}_g^n}{c\Delta t} + \mathbf{D}\cdot\boldsymbol{\nabla}\boldsymbol{\Phi}_g + \sigma_{t,g}\boldsymbol{\Phi}_g + \sigma_{\mathrm{f},g}\mathbf{F}\boldsymbol{\Phi}_g = \boldsymbol{\sigma}_g \mathbf{B}_g(T) + \boldsymbol{\sigma}_{s,g}\boldsymbol{\Phi}_g + \mathbf{S}_g. \tag{9}$$

In this equation, the superscript n designates the time step index, the absence thereof implying an implicit evaluation (i.e. at t^{n+1}). Besides, the term in red is the filtering term. We have also defined:

$$\mathbf{D} = \sum_{u \in \{x,y,z\}} \mathbf{D}_u \boldsymbol{e}_u \quad , \quad \mathbf{D}_u = \int_{4\pi} \Omega_u\, \mathbf{R}(\boldsymbol{\Omega}) \mathbf{R}^T(\boldsymbol{\Omega})\, \mathrm{d}\Omega, \tag{10}$$

$\boldsymbol{e}_x$, $\boldsymbol{e}_y$ and $\boldsymbol{e}_z$ being the (Cartesian) unit vectors and:

$$\mathbf{B}_g = \int_{4\pi} \mathbf{R}\, B_g(T) \mathrm{d}\Omega, \tag{11}$$

$$\boldsymbol{\sigma}_{\mathrm{s},g} = \mathrm{diag}\Big\{\sigma_{\mathrm{s},g,\ell}\,,\ m = -\ell, ..., \ell\,;\ \ell = 0, ..., N\Big\}, \tag{12}$$

$$\boldsymbol{\sigma}_g = \mathrm{diag}\Big\{\sigma_g\, \delta_{\ell,0}\,,\ m = -\ell, ..., \ell\,;\ \ell = 0, ..., N\Big\}, \tag{13}$$

$$\sigma_{\mathrm{s},g,\ell} = \int_{4\pi} \sigma_{s,g}\, P_\ell^0\, \mathrm{d}\Omega. \tag{14}$$

The expression of $\mathbf{F}$ is given by:

$$\mathbf{F} = \mathrm{diag}\Big\{f(\ell, N)\,,\ m = -\ell, ..., \ell\,;\ \ell = 0, ..., N\Big\}, \tag{15}$$

with the *filter function* f being:

$$f(\ell, N) \equiv -\log \rho_{\mathrm{filterType}}\left(\frac{\ell}{N+1}\right). \tag{16}$$

Although several filter types have been proposed in the past [4, 6], we only consider the following in this work:

$$\rho_{\mathrm{Lanczos}}(\zeta) \equiv \frac{\sin\zeta}{\zeta}. \tag{17}$$

The main question addressed in this paper is how to choose the value of $\sigma_{\mathrm{f},g}$ as a function g.

III. RESULTS AND ANALYSIS

1. Crooked Pipe Test Problem

We consider a common and challenging test problem for TRT applications, known as the Crooked Pipe test problem [7]. Fig. 1 describes the geometry. Initially, the entire domain is at equilibrium $T_{\mathrm{init}} = 0.05$ keV. At $t = 0$, we start applying an incoming source $T_{\mathrm{inc}} = 0.3$ keV at the left boundary for $0 \leq y \leq 0.5$ cm. The bottom boundary $y = 0$ is reflecting and all other boundaries are vacuum.

The implementation was performed within Rattlesnake, the Idaho National Laboratory transport solver based on the Multiphysics Object Oriented Simulation Environment (MOOSE) finite element framework [8].

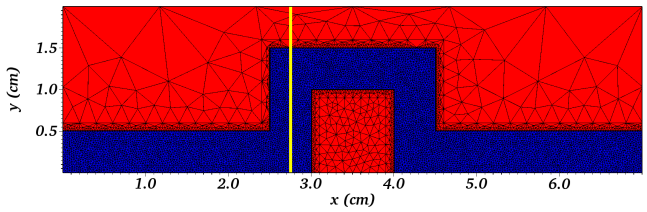

Fig. 1: Geometry of the Crooked Pipe test problem: the value for σ_0 is chosen such that the opacity $\sigma_{g=3}(T = 0.05\,\text{keV})$ is equal to 200 cm^{-1} and 0.2 cm^{-1} in the red and blue regions, respectively. In addition, the heat capacity respectively is 0.5 and $5{\times}10^{-4}$ $\text{GJ/cm}^4\text{/keV}$. The 20106-element mesh is also displayed. Results along the straight line $x = 2.75$ cm in yellow will be presented in Fig. 3 and Table III.

2. Energy Structure

Because the study of that problem for gray FP_N calculations has been studied in detail in [5], we wish to create an energy structure that will induce a different behavior in each group, so that we can study how to adjust $\sigma_{\text{f},g}$ when the need for filtering is group-dependent.

A 4-group energy structure is proposed in Table I and is believed to be relevant because the incoming source emits mostly in the *fast* groups ($g = 3, 4$) while the Planckian re-emission – at least at early times – mostly occurs in the *thermal* groups ($g = 1, 2$). Since the negative regions typically appear when strong variations in angle are present in the solution, it is therefore expected to need a stronger filter in the *fast* groups (the re-emission being isotropic and thus smooth in angle).

The number of groups $G = 4$ is chosen such that it would be inconvenient to adjust the filter strength in each group individually but is kept fairly low because of our model opacity, which would cause some groups to be essentially optically transparent if we were to choose more groups. Note however that the methodology presented below is not restricted to low values of G.

T (keV)	$g = 1$	$g = 2$	$g = 3$	$g = 4$
$T_{\text{init}} = 0.05$	18.11%	67.90%	13.98%	0.01%
$T_{\text{inc}} = 0.3$	0.17%	3.29%	43.00%	53.54%

TABLE I: Proportion of the radiation emitted in each group for different temperatures. The bounds for the energy group are 0.001, 0.1, 0.3, 1 and 10 keV.

3. Multigroup Opacities

We compute the Rosseland-averaged opacities for the aforementioned 4-group energy structure. We choose σ_0 (cf Eq. (5)) such that the opacity for $g = 1$ and $g = 4$ is not excessively thick and thin, respectively. The actual choice is described in Fig. 1.

Table II then gives the opacities for the different energy groups in the thin region for various values of the temperature. The opacities in the thick region are 1,000 times higher (for a given group).

A power regression on the data from Table II gives:

$$\sigma_{g=1}(T) = 2.905\,T^{-0.7197}, \tag{18}$$

$$\sigma_{g=2}(T) = 0.3210\,T^{-0.4857}, \tag{19}$$

$$\sigma_{g=3}(T) = 0.006617\,T^{-1.0502}, \tag{20}$$

$$\sigma_{g=4}(T) = 0.0006914\,T^{-1.0550}, \tag{21}$$

with the coefficients of determination for each group being equal to $R^2_{g=1} = 0.994$, $R^2_{g=2} = 0.996$, $R^2_{g=3} = 0.949$, $R^2_{g=4} = 0.920$ respectively, where T is expressed in keV and σ in cm^{-1}. In practice, the temperature is lagged for the evaluation of these opacities (to accelerate the solver convergence).

4. Filter Strength

A. Filtering Strategy: Planck-weighted Filter Strength

We propose the following method to determine $\sigma_{\text{f},g}$ as a function of the energy group, which essentially requires as much work as its determination in the gray case:

- Run an unfiltered calculation to see where the negative regions appear – typically the edge of shadows.
- Determine the filter strength in the group that has the strongest negativity. In our case, it would be $\tilde{g} = 4$. A good value is $\sigma_{\text{f},4} = 100\ \text{cm}^{-1}$. Note that this is twice as large as what we chose in the gray case; this is because the problem tend to be more 'negative', as explained above.
- Determine the filter strengths in the other groups using:

$$\sigma_{\text{f},g} \equiv T_{\text{ref}} \frac{B_g(T_{\text{ref}})}{B_{\tilde{g}}(T_{\text{ref}})} \sigma_{\text{f},\tilde{g}}, \tag{22}$$

  where T_{ref} is a reference temperature characterizing the intensity of the driving source causing the negativity. In our case, $T_{\text{ref}} = 0.3$ keV seems to be an appropriate choice.

  The intuition behind this formula is that, looking at Table I, we will need less filtering for the thermal groups since very little of the incoming radiation takes place in these groups.

For the problem presented above, choosing $\sigma_{\text{f},4} = 100\ \text{cm}^{-1}$ removes most of the negativity in that group. The filter strength in each group is then given by (using Eq. (22)):

$$\sigma_{\text{f},1} = 0.3\ \text{cm}^{-1} \quad , \quad \sigma_{\text{f},2} = 6.1\ \text{cm}^{-1} \tag{23}$$

$$\sigma_{\text{f},3} = 80\ \text{cm}^{-1} \quad , \quad \sigma_{\text{f},4} = 100\ \text{cm}^{-1} \tag{24}$$

It is noted that these values are not as huge as they may a priori seem, compared to the opacities in Table II. Indeed, in Eq. (9), $\sigma_{\text{f},g} f(\ell, N)$ plays the role of an opacity (not just $\sigma_{\text{f},g}$): for instance, the contribution in the equations corresponding to $\ell = 1$ in a P_3 calculation is $f(1,3)\sigma_{\text{f},g} \approx 0.01\sigma_{\text{f},g}$ and it further decreases as N increases.

Temperature T (keV)	$g = 1$	$g = 2$	$g = 3$	$g = 4$
0.05	2.316E+1	1.383E+0	2.000E-1	1.135E-2
0.06	2.114E+1	1.233E+0	1.546E-1	1.082E-2
0.07	1.944E+1	1.140E+0	1.206E-1	1.029E-2
0.08	1.799E+1	1.073E+0	9.638E-2	9.744E-3
0.09	1.673E+1	1.022E+0	7.940E-2	9.199E-3
0.1	1.562E+1	9.788E-1	6.749E-2	8.656E-3
0.11	1.465E+1	9.415E-1	5.899E-2	8.121E-3
0.12	1.379E+1	9.081E-1	5.279E-2	7.596E-3
0.13	1.302E+1	8.775E-1	4.817E-2	7.086E-3
0.14	1.233E+1	8.493E-1	4.463E-2	6.595E-3
0.15	1.171E+1	8.229E-1	4.186E-2	6.125E-3
0.16	1.115E+1	7.982E-1	3.965E-2	5.679E-3
0.17	1.064E+1	7.748E-1	3.785E-2	5.257E-3
0.18	1.017E+1	7.528E-1	3.636E-2	4.861E-3
0.19	9.742E+0	7.319E-1	3.510E-2	4.490E-3
0.2	9.347E+0	7.120E-1	3.403E-2	4.145E-3
0.21	8.983E+0	6.932E-1	3.310E-2	3.826E-3
0.22	8.646E+0	6.752E-1	3.228E-2	3.530E-3
0.23	8.333E+0	6.582E-1	3.155E-2	3.257E-3
0.24	8.041E+0	6.419E-1	3.090E-2	3.006E-3
0.25	7.769E+0	6.263E-1	3.031E-2	2.776E-3
0.26	7.515E+0	6.114E-1	2.978E-2	2.565E-3
0.27	7.277E+0	5.972E-1	2.928E-2	2.371E-3
0.28	7.053E+0	5.836E-1	2.882E-2	2.194E-3
0.29	6.843E+0	5.706E-1	2.839E-2	2.031E-3
0.3	6.645E+0	5.581E-1	2.798E-2	1.882E-3

TABLE II: Temperature-dependent opacities for the 4-group Crooked Pipe in cm^{-1} in the thin region. The opacities in the thick region are 1,000 times larger.

B. Spatial Strategy: Uniform vs Local Filtering

We have shown in [5] for gray calculations that having a spatially dependent filter can help converge faster to the reference solution by only turning the filter on where it is needed. Practically, it need be activated where negative regions for unfiltered calculations appear along with upstream regions of a comparable size [5]. Fig. 2 shows what such a profile looks like for the Crooked Pipe test problem.

Admittedly, it would be ideal to come up with an efficient way to determine this filter spatial dependency automatically. Unfortunately – and that is probably the main flaw of the method, attempts to do so have resulted in much more computationally expensive methods. This is in particular due to the fact that activating the filter only in regions where the scalar flux tends to become negative is typically not enough (as we mentioned, upstream regions of a comparable size need usually be included, too). That being said, it is believed that the guidelines presented above are fairly general. For more detailed directions, the interested reader may refer to [5] and also keep in mind that the filter strength may be adjusted on coarse meshes.

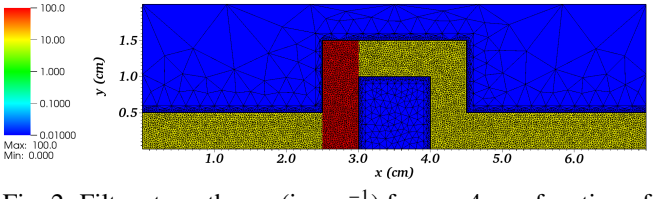

Fig. 2: Filter strength $\sigma_{f,g}$ (in cm^{-1}) for $g = 4$ as a function of space for the local filtering strategy.

5. Results

Fig. 3 shows the results for $\Phi^0_{0,g=4}$ for the different filtering strategies along the straight line $x = 2.75$ cm at $t = 0.035$ sh, time around which the unfiltered solution reaches its most negative values. The uniformly filtered P_{39} is used as a reference. The negative values and oscillatory behavior of the unfiltered solution clearly appear in Fig. 3a. While the uniform filtering strategy indeed removes the negativity from the solution, as shown in Fig. 3b, convergence to the reference solution is attained faster with local filtering (Fig. 3c).

Quantitative results showing the L2-error for each filtering strategy as a function of N are presented in Table III.

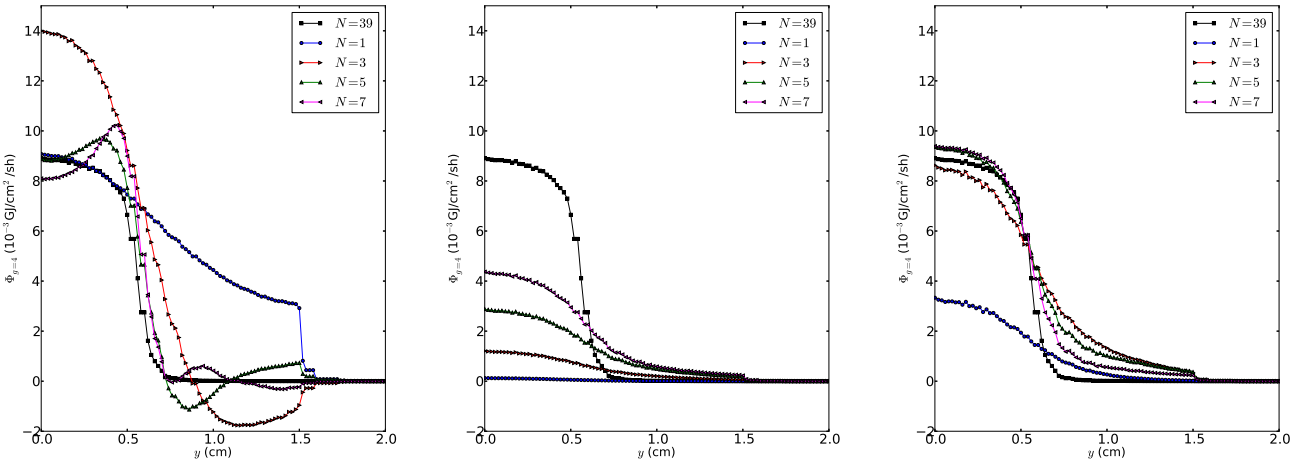

(a) Unfiltered (b) Uniform (c) Local

Fig. 3: Scalar flux $\Phi^0_{0,g=4}$ along the straight line $x = 2.75$ cm at $t = 0.035$ sh for different filtering strategies. The values for $\sigma_{\mathrm{f},g}$ are given by Eqs. (23) and (24). For the local filtering, the spatial dependency in each group is given by Fig. 2.

	Unfiltered	Uniform	Local
P_1	4.278E-3	6.155E-3	4.139E-3
P_3	3.809E-3	5.440E-3	1.637E-3
P_5	1.103E-3	4.324E-3	1.286E-3
P_7	1.305E-3	3.351E-3	8.520E-4

TABLE III: L2-error of $\Phi^0_{0,g=4}$ in GJ-cm$^{-3/2}$-sh^{-1} along $x = 2.75$ cm at $t = 0.035$ sh. This is computed by computing the L2-error of each curve on Fig. 3 with respect to the P_{39} solution.

6. Computational Cost

In this section, we are interested in the computational cost of the method as a function of the filter strength and the spatial filtering strategy. Fig. 4 displays the number of linear iterations required by the GMRES solver for the first time step – which is also the most expensive – as a function of the filter strength. It in particular exhibits a behavior very similar to that found for gray calculations: for uniform filtering the number of linear iterations decreases as $\sigma_{\mathrm{f},\tilde{g}}$ increases and converges to a number independent of N. For a local filtering strategy, the number first decreases before increasing and converging to a constant value. In both cases, the computational cost is noticeably reduced for the practical value of $\sigma_{\mathrm{f},\tilde{g}}$ used (by more than 40% and 25% respectively, for $N \geq 3$).

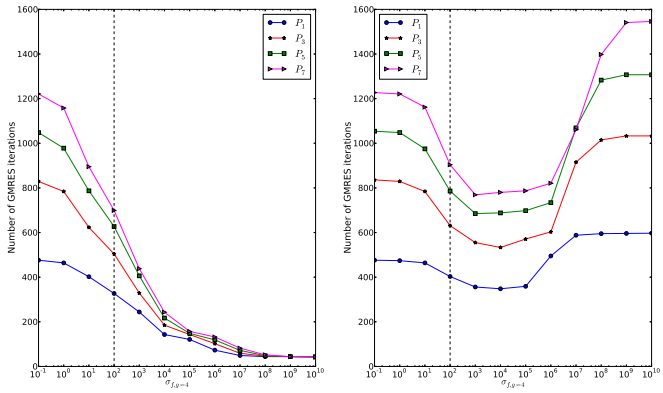

Fig. 4: Number of linear iterations for the first time step as a function of N and the filter strength $\sigma_{\mathrm{f},\tilde{g}}$ (in cm^{-1}). As a reference, the value of $\sigma_{\mathrm{f},\tilde{g}}$ for this test problem was in practice chosen to be 100 cm^{-1} (vertical dotted line). For the local filter, $\sigma_{\mathrm{f},\tilde{g}}$ designates the maximum value.

IV. CONCLUSIONS

In summary, we have presented an extension of the Implicit Filtered P_N method to multigroup calculations for TRT applications which can be successfully used to reduce the oscillations and negativity induced by the P_N approximation. While the filter strengths a priori need be adjusted in each

group individually, we have suggested a method relying on weighting them using the planckian distribution evaluated at the driving temperature responsible for the negativity. Though this approach may not be universally suited to more complicated problems, where determining such a temperature may not be straightforward, it allows for a simple method, practically requiring no more work than for gray calculations. Only one filter strength then has to be adjusted, which can be done on coarse meshes. Furthermore, similarly to what was observed for energy-independent filtering, the computational cost of the method tends to be reduced by the filter. This constitutes an additional advantage compared to an unfiltered P_N approach.

V. ACKNOWLEDGMENTS

This material is based upon work supported by the National Science Foundation under Grant No. 1217170.

REFERENCES

1. M. L. ADAMS and P. F. NOWAK, "Asymptotic Analysis of a Computational Method for Time- and Frequency-Dependent Radiative Transfer," *Journal of Computational Physics*, **146**, 366–403 (1998).
2. RYAN G. MCCLARREN, CORY D. HAUCK, "Robust and accurate filtered spherical harmonics expansions for radiative transfer," *Journal of Computational Physics*, **229**, 5597–5614 (2010).
3. CORY AHRENS, SIMON MERTON, "An improved filtered spherical harmonic method for transport calculations," *Proceedings of International Conference on Mathematics, Computational Methods & Reactor Physics, Sun Valley, Idaho, May 5-9, 2013*.
4. DAVID RADICE, ERNAZAR ABDIKAMALOV, LUCIANO REZZOLLA, CHRISTIAN D. OTT, "A new spherical harmonics scheme for multi-dimensional radiation transport I. Static matter configurations," *Journal of Computational Physics*, **242**, 648–669 (2013).
5. V. M. LABOURE, R. G. MCCLARREN, and C. D. HAUCK, "Implicit Filtered P_N for High-Energy Density Thermal Radiation Transport using Discontinuous Galerkin Finite Elements." *Journal of Computational Physics*, **321**, 624–643 (2016).
6. MARTIN FRANK, CORY HAUCK, AND KERSTIN KUEPPER, "Convergence of Filtered Spherical Harmonic Equations for Radiation Transport," *Communications in Mathematical Sciences*, **14**, 1443–1465 (2016).
7. F. GRAZIANI and J. LEBLANC, Tech. Rep. UCRL-MI-143393 (2000).
8. D. GASTON, C. NEWMAN, G. HANSEN, and D. LEBRUN-GRANDIÉ, "MOOSE: A Parallel Computational Framework for Coupled Systems of Nonlinear Equations," *Nuclear Engineering and Design*, **239**, *10*, 1768–1778 (2009).